 doi:10.20944/preprints202010.0616.v1

Article

Statistical model-based classification to detect patient-specific spike-and-wave in EEG signals

Antonio Quintero-Rincón [1,2,3]* 0000-0003-0186-4049, Valeria Muro[2], Carlos D'Giano [2], Jorge Prendes [3] 0000-0002-1570-2115, and Hadj Batatia [4] 1111-2222-3333-4444

1 Departament of Electronic, Catholic University of Argentina (UCA), Buenos Aires, Argentina; antonioquintero@uca.edu.ar
2 Foundation for the Fight against Pediatric Neurological Disease (FLENI), Buenos Aires, Argentina cmuro@fleni.org.ar, cdigiano@fleni.org.ar
3 IRIT-INPT-ENSEEIHT, University of Toulouse, Toulouse, France; jorge.prendes@tesa.prd.fr
4 MACS school, Herriot Watt University, Dubai Campus; h.batatia@hw.ac.uk
* Correspondence: antonioquintero@uca.edu.ar

Abstract: Spike-and-wave discharge (SWD) pattern detection in electroencephalography (EEG) is a crucial signal processing problem in epilepsy applications. It is particularly important for overcoming time-consuming, difficult, and error-prone manual analysis of long-term EEG recordings. This paper presents a new method to detect SWD, with a low computational complexity making it easily trained with data from standard medical protocols. Precisely, EEG signals are divided into time segments for which the continuous Morlet 1-D wavelet decomposition is computed. The generalized Gaussian distribution (GGD) is fitted to the resulting coefficients and their variance and median are calculated. Next, a *k*-nearest neighbors (*k*-NN) classifier is trained to detect the spike-and-wave patterns, using the scale parameter of the GGD in addition to the variance and the median. Experiments were conducted using EEG signals from 6 human patients. Precisely, 106 spike-and-wave and 106 non-spike-and-wave signals were used for training, and 96 other segments for testing. The proposed SWD classification method achieved 95 % sensitivity (True positive rate), 87% specificity (True Negative Rate), and 92% accuracy. These promising results set the path for new research to study the causes underlying the so-called *absence epilepsy* in long-term EEG recordings.

Keywords: Spike-and-wave; Generalized Gaussian distribution; EEG; Morlet wavelet; *k*-nearest neighbors classifier; Epilepsy

1. Introduction

Epilepsy is a chronic neurological disorder that affects patients, causing recurrent seizures. Seizures are characterized by excessive electrical discharges in neurons. Their waveform known as the spike is characterized by brief bursts of high amplitude , synchronized and multiphasic activity with several polarity changes [1]. These are exhibited close to the epileptic focus and stand out from the background EEG activity. Electroencephalography (EEG) is currently the main technique to record electrical activity in the brain. Neurologists, trained in EEG, are able to properly determine an epilepsy diagnosis by analyzing the different types of spikes in the so-called *rhythmic activity* of the brain.

Existing, automatic methods for detecting epileptic events in EEG signals have performance that greatly exceed visual inspection. These methods focus mostly on interictal spikes [2,3], seizure onset detection [4], or waveform epileptic patterns [5,6]. There exists a wide variety of methods to accurately detect seizures and their patterns in EEG. Most of these methods are based on supervised machine learning techniques, such as Support Vector Machine [7], logistic regression [8], decision trees [9], *k*-Nearest Neighbor, Random Forest [10], or discriminant analysis [11]. They mainly differ according to their feature extraction and classification approaches. A large variety of features are used including spatio-temporal analysis [12], spectral-temporal analysis [13], wavelet decomposition [2], spectrogram

 doi:10.20944/preprints202010.0616.v1

[14,15], Hilbert transform [16], neural networks [17], Hurst exponent [18], quadratic linear-parabolic model [19], and statistical descriptors such as statistical modeling [20], signal fuzzy entropy [21], and fractal dimension [22]. The reader is referred to [23] for a recent state-of-the-art on methods for seizure detection in EEG.

Spike-and-wave discharge (SWD) is a generalized EEG discharge pattern, where the waveform has a regular and symmetric morphology. This morphology can be mathematically described by a Morlet wavelet transform, generating a time-frequency representation of the EEG signal [24–27]. The *spike* component of an SWD is associated with neuronal firing and the *wave* component is associated with neuronal inhibition or hyperpolarization of neurons [28]. SWD is widely used in mice studies [2, 14,29,30]; inversely, the literature reports very limited human applications. Mice have a predisposition for generalized SWD at 7-12 Hz [15] and typically have spontaneous absence-seizure-like events. Rodent models are usually used to study the neurobiological mechanisms underlying SWD in humans. However, studies in humans and rodents differ in the way SWD is assessed and, more importantly, rodents and humans show substantial biological differences. Thus more human studies are necessary to fully understand this phenomena. This paper fits in this general aim by studying SWD in human.

Some recent works have been proposed to estimate SWD patterns in human using machine learning techniques. They rely on different models and features, including 1-NN with t-location-scale distribution [20], decision-trees with cross-correlation coupled with decision trees [9], and Bayesian classifiers with the Walsh transformation [33]. Table 1 lists some more methods. Other existing methods implement signal analysis techniques, such as Hilbert-Huang transform to analyse time-frequency energy distribution [34], complex network of neuronal oscillators to model SWD [35], analysing statistical features such as variance, sum of wave amplitudes, slope of wave [36], or topographic cluster analysis based on connectivity, entropy, frequency, power, and spike amplitude [37]. For a biological dynamic explanation of features and mechanisms generating SWD in the brain see [38].

Table 1. Some state-of-the-art methods for the SWD estimation in EEG signals in humans, compared in terms of classification techniques, features, and reported performance.Abbreviations are as follows: high Specificity, rule in (SpPIn), According to the frequency and magnitude weighted average (WA), According to an estimated threshold (AET)

Method	Features	Classifier	Accuracy in %	Ref.
Generalized Gaussian distribution (GGD)	GGD parameters, variance and median from time-frequency Morlet decomposition	10-NN	92	our
Kendall's Tau-b Coefficient	Kendall's Tau-b coefficient significance	SpPIn	94	[39]
Ramanujan Filter Bank (RFB)	Spectrum from RFB	Empirical	> 80	[40]
t-location-scale distribution (TLS)	TLS parameters	1-NN	100	[20]
Cross-correlation	Correlation coefficient	Decision trees	97	[9]
Walsh transformation (WT)	First and second orden from WT	Bayesian	> 70	[33]
Hilbert-Huang transform	Intrinsic mode functions energy	WA	-	[34]
Cross-correlation	Wavelet spectrum correlation	AET	100	[41]

This paper presents a new SWD patient-specific detection method based on the statistical modeling of the continuous Morlet wavelet coefficients. Precisely, we fit the generalized Gaussian distribution to these coefficients and estimate the corresponding parameters. These parameters are used as features in a 10-NN classifier. Training and testing of the learning model use different EEG datasets.

The remainder of the paper is structured as follows. Section 2 presents the EEG database, and the proposed methodology, where we explain the continuous Morlet wavelet transformation, the generalized Gaussian distribution (GGD) statistical model, and the k-NN classifier. Experimental results using the *scale* parameter from the GGD and the *variance* and *median* from the continuous

Preprints (www.preprints.org) | NOT PEER-REVIEWED | Posted: 29 October 2020 doi:10.20944/preprints202010.0616.v1

wavelet coefficients are reported in section 3, flowed by discussion in section 4. Conclusions, remarks, and perspectives are presented in Section 5.

2. Materials and Methods

This section presents our statistical model-based method to detect spike-and-wave discharges (SWD) in EEG signals. It is computationally very efficient, suitable for real-time implementation, allowing on-line spike-and-wave detection. First, we describe the dataset used for experimentation, then we present the different processing steps.

2.1. Database

A standard 10/20 EEG systems was used at the Foundation for the Fight against Pediatric Neurological Disease (FLENI) to acquire long term 256Hz EEG signal, from 12 human patients. The following 22-channels were used: Fp1, Fp2, F7, F3, Fz, F4, F8, T3, C3, Cz, C4, T4, T5, P3, Pz, P4, T6, O1, O2, Oz, FT10 and FT9. See [39] for more details. The acquired signals had different waveform and duration.

All EEG signals were labeled by a neurologist from FLENI to indicate the onset and duration of the epilepticform. Based on these annotations, we extracted 212 short epochs (1-minute average duration) focusing on the spike-and-wave waveform. As such, a database with the 212 monopolar signal epochs was created, with 106 SWD signals and 106 non-SWD signals. Each SWD signal has been restricted to a narrow frequency band between 1-3 Hz. Figure 1 shows an example of a typical SWD signal. Visually, one can observe that SWD patterns exhibit characteristic morphology; whereas non-SWD signals have normal waveform.

Six patients with twenty (20) signals each were used for training our predictive model (Section 2.2). This multiplicity of signals from the same patient has been decided to enforce learning-patient specific patterns. A set of 96 signals from the other 6 patients were used for testing.

2.2. Methodology

The proposed method composes of four stages. The first stage divides every EEG signal epoch, $\boldsymbol{X} \in \mathbb{R}^{N \times M}$ with M channels and N time instants, into 2-second segments per channel, with 1-second overlap across a rectangular sliding window. Please note that M is fixed to 22, whereas N varies for different epochs (with an average duration of 60 seconds giving about $N = 256 * 60 = 15360$ samples). This will give $[N/60]$ segments per channel. The second stage consists in applying Morlet decomposition to create separate time-frequency representation for each segment $\boldsymbol{X}_t \in \mathbb{R}^{N \times 1}$. The purpose of this decomposition is to evaluate the energy distribution throughout the SWD frequency band (1-3 Hz). In the third stage, the statistical distribution of the wavelet coefficients from each segment is represented using a zero-mean generalized Gaussian distribution (GGD). A maximum likelihood method is used to estimate the GGD parameters, *scale* (ς) and *shape* (τ) [4,42–44]. This statistical modeling stage gives $M \times [N/60]$ pairs of *scale* (ς) and *shape* (τ) parameters, achieving a very strong dimension reduction. As we demonstrate it in the experimentation section, the scale parameter ς was found statistically characteristic of SWD waveform, and it is proposed as a feature to detect such patterns [4,44]. Using a single parameter to classify patterns is too strict and misses the natural variability in the data. For this reason, we compute two other statistical parameters, namely the *variance* (σ^2) and the *median* ($\widetilde{x}$) from the wavelet coefficients of each segment. The data from one EEG epoch reduces therefore to three parameters, $\{\varsigma, \sigma^2, \widetilde{x}\}$, giving a high dimension reduction while offering a flexible representation space to discriminate patterns while accounting for natural variability. Please note, in total we will have $M \times [N/60] * 3$ parameters for any EEG signal epoch. Finally, a classification model has been trained to detect SWD patterns, using the three features parameters. The proposed methodology is summarized in Figure 2. The following sections describe each stage.

Preprints (www.preprints.org) | NOT PEER-REVIEWED | Posted: 29 October 2020 doi:10.20944/preprints202010.0616.v1

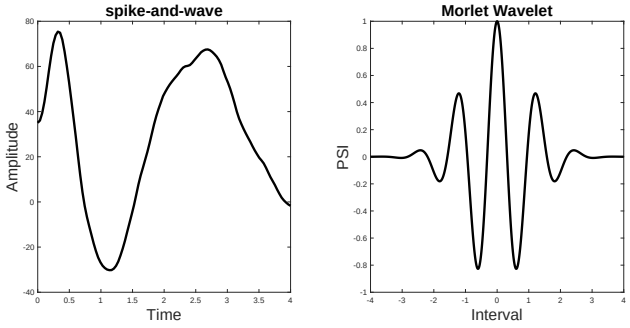

(a) SWD and Morlet Wavelet

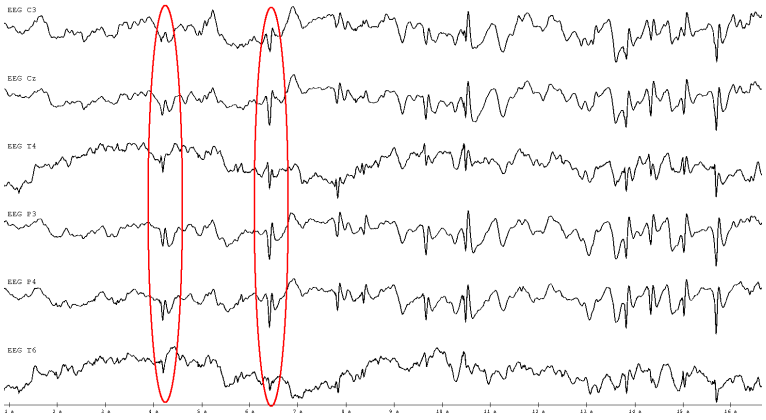

(b) EEG example

Figure 1. (**a**)A sample SWD signal and the Morlet wavelet. Note that the scales are different. (**b**) Example of 6 channels of one monopolar raw EEG, with SWD patterns in all channels.

We now introduce the Morlet wavelet, the Generalized Gaussian distribution, and the k-nearest neighbors classifier used in this paper.

2.2.1. Morlet Wavelet

The continuous wavelet transform is given by

$$W_f(t,a,b) = \int_{-\infty}^{\infty} \mathbf{X}_t \; \psi^*_{a,b}(t)\mathrm{dt} \tag{1}$$

$$\psi^*_{a,b}(t) = \frac{1}{\sqrt{a}} \; \psi\left(\frac{t-b}{a}\right) \tag{2}$$

$$\psi(t) = \exp^{-\frac{t^2}{2}} \; cos(5t) \tag{3}$$

where a is the scaling parameter and b the shift parameter. Equation (2) is the mother wavelet function, where $(*)$ denotes the complex conjugate operation. Equation (3) is the analytic expression of the Morlet wavelet [45]. In order to use the Morlet wavelet with frequency f_c, we use the relationship

$$f_a = \frac{f_c}{\alpha\Delta} \tag{4}$$

where α is the scale, Δ is the sampling period, f_c is the center frequency of Morlet wavelet (in Hz) and f_a is the pseudo-frequency corresponding to the scale a (in Hz). As such, the wavelet dominant frequency can be characterized using the center frequency, as it detects the main wavelet oscillations (the reader is referred to [46] for details). Note that the wavelet scale is estimated according to the narrow frequency 1-3 Hz from (Section 2.1). In our case, $\Delta = 256$, and $1 < frequency < 3$, we have a

Preprints (www.preprints.org) | NOT PEER-REVIEWED | Posted: 29 October 2020 doi:10.20944/preprints202010.0616.v1

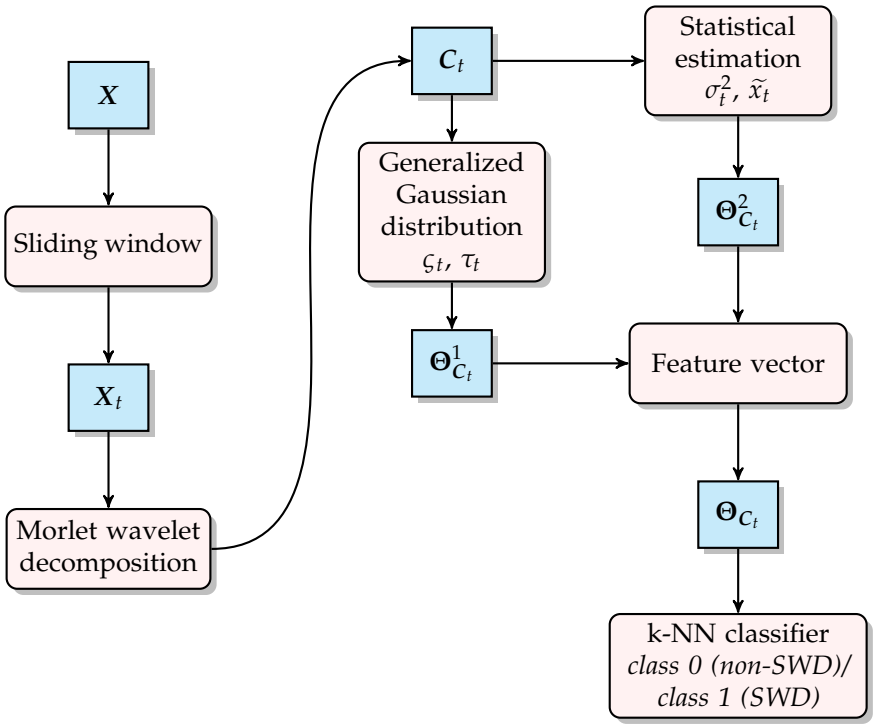

Figure 2. Diagram of the proposed method

scale $\alpha \in fc * \Delta, fc * \Delta/3$. Figure 3 show an example of time-scale variation for a value of $f_c = 1.2308$ for SWD and $f_c = 0.8125$ for non-SWD. These data are from signal 1 from patient 1.

2.2.2. Generalized Gaussian distribution

The generalized Gaussian distribution (GGD) is a flexible statistical model often used in science and engineering to represent data. We propose to represent the distribution of the Morlet wavelet coefficients ($\boldsymbol{C}_t$) using the GGD [47]. The probability density function (PDF) of the GGD is given by the expression

$$f_{\mathrm{GGD}}(x;\varsigma,\tau) = \frac{\tau}{2\varsigma\Gamma(\tau^{-1})} \exp\left(-\left|\frac{x}{\varsigma}\right|^{\tau}\right) \tag{5}$$

where $\varsigma \in \mathbb{R}^+$ is a scale parameter, $\tau \in \mathbb{R}^+$ is a shape parameter, and $\Gamma(\cdot)$ is the Gamma function. Fitting equation (5) to the data $\boldsymbol{C}_t$ is performed using the maximum likelihood estimators $\boldsymbol{\Theta}^1_{C_t}$:

$$\boldsymbol{\Theta}^1_{C_t} = [\varsigma_t, \tau_t]^T = \underset{[\varsigma,\tau]^T}{\arg\max}\, f_{\mathrm{GGD}}(\boldsymbol{C}_t;\varsigma,\tau) \tag{6}$$

For more details about the estimation of the GGD parameters, we refer the reader to our previous work [4,42–44,48].

2.2.3. Feature parameters

Through the previously described stages, data from every signal epoch, $M \times N$ samples, is reduced to the matrix of parameters (or features) $\boldsymbol{\Theta}_{C_t}$, composed of $M \times [N/60]$ rows, with three columns consisting of our data is reduced to the matrix of parameters (or features) $\boldsymbol{\Theta}_{C_t}$, composed of the *scale* parameter from the GGD, the variance and the median of the Morlet wavelet coefficients.

$$\boldsymbol{\Theta}_{C_t} = [\varsigma_t, \sigma_t^2, \widetilde{x}_t] \tag{7}$$

Preprints (www.preprints.org) | NOT PEER-REVIEWED | Posted: 29 October 2020 doi:10.20944/preprints202010.0616.v1

Using this representation, the next stage consists in training a k-nearest neighbors classifier to detect SWD patterns. Please, recall that we have 212 signal epochs in our database. All went through the preceding dimension reduction process. A set of 120 of those (from 6 patients) will serve for training and the remaining 96 (from 6 other patients) are used for testing.

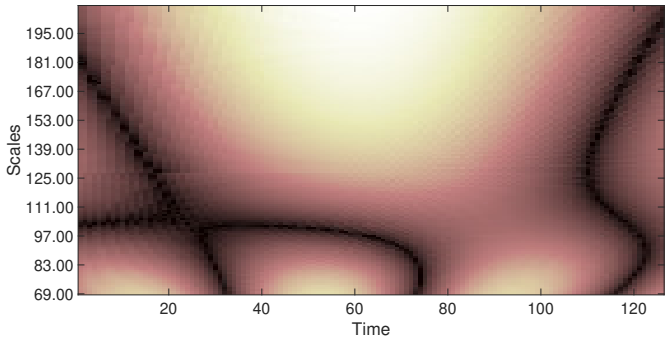

(a) SWD

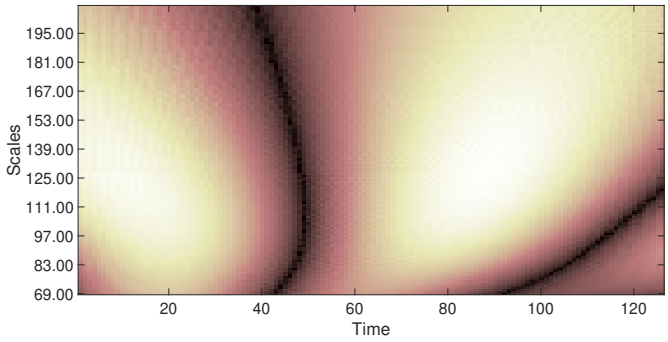

(b) non-SWD

Figure 3. Illustration of the variation of time-scale for Morlet continuous wavelet (**a**) for SWD with $f_c = 1.2308$ Hz, and(**b**) for non-SWD with $f_c = 0.8125$. Note that, the energy distribution pattern is different when comparing SWD and non-SWD.

2.2.4. $K-$nearest neighbors classification

Using the feature vector $\mathbf{\Theta}_{C_t}$, consider a classification into two possible classes $c = 0$ (non-SWD) and $c = 1$ (SWD). The probability of classifying a sample in one of the two classes is given by

$$\begin{aligned}
\rho\left(\mathbf{\Theta}_{C_t}|c=0\right) &= \frac{1}{N_0}\sum_{n\in\text{class }0}\mathcal{N}\left(\mathbf{\Theta}_{C_t}|\mathbf{\Theta}^n_{C_t},\sigma^2\boldsymbol{I}\right)\\
&= \frac{1}{N_0\left(2\pi\sigma^2\right)^{D/2}}\sum_{n\in\text{class }0}\exp^{-\frac{\left(\mathbf{\Theta}_{C_t}-\mathbf{\Theta}^n_{C_t}\right)^2}{2\sigma^2}} \qquad (8)\\
\rho\left(\mathbf{\Theta}_{C_t}|c=1\right) &= \frac{1}{N_1}\sum_{n\in\text{class }1}\mathcal{N}\left(\mathbf{\Theta}_{C_t}|\mathbf{\Theta}^n_{C_t},\sigma^2\boldsymbol{I}\right)\\
&= \frac{1}{N_1\left(2\pi\sigma^2\right)^{D/2}}\sum_{n\in\text{class }1}\exp^{-\frac{\left(\mathbf{\Theta}_{C_t}-\mathbf{\Theta}^n_{C_t}\right)^2}{2\sigma^2}} \qquad (9)
\end{aligned}$$

Preprints (www.preprints.org) | NOT PEER-REVIEWED | Posted: 29 October 2020 doi:10.20944/preprints202010.0616.v1

where D is the dimension of the sammple $\mathbf{\Theta}_{C_t}$, N_0 and N_1 are the numbers of training samples from class 0 and class 1, respectively; and σ^2 is the variance. Using the Bayes rule to classify a new observation $\mathbf{\Theta}^*_{C_t}$, we obtain the following equation

$$\rho\left(c=0|\mathbf{\Theta}^*_{C_t}\right)=\frac{\rho\left(\mathbf{\Theta}^*_{C_t}|c=0\right)\rho\left(c=0\right)}{\rho\left(\mathbf{\Theta}^*_{C_t}|c=0\right)\rho\left(c=0\right)+\rho\left(\mathbf{\Theta}^*_{C_t}|c=1\right)\rho\left(c=1\right)} \tag{10}$$

The maximum likelihood gives $\rho(c=0)=N_0/(N_0+N_1)$, and $\rho(c=1)=N_1/(N_0+N_1)$. Substituting in equation (10), we obtain the probability $\rho\left(c=0|\mathbf{\Theta}^*_{C_t}\right)$. The expression for $\rho\left(c=1|\mathbf{\Theta}^*_{C_t}\right)$ can be derived in a similar manner. To determine which class is most likely, the ratio between the two expressions is evaluated

$$\frac{\rho\left(c=0|\mathbf{\Theta}^*_{C_t}\right)}{\rho\left(c=1|\mathbf{\Theta}^*_{C_t}\right)}=\frac{\rho\left(\mathbf{\Theta}^*_{C_t}|c=0\right)\rho\left(c=0\right)}{\rho\left(\mathbf{\Theta}^*_{C_t}|c=1\right)\rho\left(c=1\right)} \tag{11}$$

If the ratio is greater than one, $\mathbf{\Theta}^*_{C_t}$ is classified as $c=0$, otherwise it is classified as $c=1$. It is important to note that in the case where σ^2 is very small in (11), then both the numerator and denominator will be dominated by the term for which the sample $\mathbf{\Theta}^{n_0}_{C_t}$ in class-0 or $\mathbf{\Theta}^{n_1}_{C_t}$ in class-1 are closest to the point $\mathbf{\Theta}^*_{C_t}$, such that

$$\begin{aligned}\frac{\rho\left(c=0|\mathbf{\Theta}^*_{C_t}\right)}{\rho\left(c=1|\mathbf{\Theta}^*_{C_t}\right)}&=\frac{exp^{-\frac{\left(\mathbf{\Theta}^*_{C_t}-\mathbf{\Theta}^{n_0}_{C_t}\right)^2}{2\sigma^2}}\rho\left(c=0\right)/N_0}{exp^{-\frac{\left(\mathbf{\Theta}^*_{C_t}-\mathbf{\Theta}^{n_1}_{C_t}\right)^2}{2\sigma^2}}\rho\left(c=1\right)/N_1}\\&=\frac{exp^{-\frac{\left(\mathbf{\Theta}^*_{C_t}-\mathbf{\Theta}^{n_0}_{C_t}\right)^2}{2\sigma^2}}}{exp^{-\frac{\left(\mathbf{\Theta}^*_{C_t}-\mathbf{\Theta}^{n_1}_{C_t}\right)^2}{2\sigma^2}}}\end{aligned} \tag{12}$$

On the limit $\sigma^2\to 0$, $\mathbf{\Theta}^*_{C_t}$ is classified as class 0 if $\mathbf{\Theta}^*_{C_t}$ has a point in the class 0 data which is closer than the closest point in the class 1 data. The nearest neighbor method is therefore recovered as the limiting case of a probabilistic generative model. The parameter k is chosen based on $\sqrt{N}$, where N is the number of samples in the training dataset. We refer the reader to [49,50] for a comprehensive treatment of the mathematical properties of k-nearest neighbors classifier.

3. Results

The annotated database introduced in Section 2.1 was used to compute the feature vector $[\varsigma_t,\sigma_t^2,\widetilde{x_t}]\in\mathbb{R}^3$, based on the statistical model of the coefficients of the continuous Morlet wavelet. The resulting features were used for off-line training the k-nearest neighbor classifier. With the 212 samples, k was set to 10 giving a $10-$nearest neighbour.

Tables 2 to 4 show the statistical mean, standard deviation, variance and bounds values from the feature vector. One can note that, sigma (ς_t), variance (σ_t^2), and median ($\widetilde{x_t}$) are larger for SWD that for non-SWD. Therefore, despite the overlapping statistical bounds, a threshold can be determined to detect SWD patterns.

Table 2. Mean, standard deviation, variance and bound values for sigma parameter (ς) for class 0 (non-spike-and-wave) and class 1 (spike-and-wave).

	Mean	std	Variance	Bounds
Class 0	293	267.8017	71718	[12,1275]
Class 1	542	406.2597	165047	[31, 1811]

Preprints (www.preprints.org) | NOT PEER-REVIEWED | Posted: 29 October 2020 doi:10.20944/preprints202010.0616.v1

Table 3. Mean, standard deviation, variance and bound values for the variance (σ_t^2) for class 0 (non-spike-and-wave) and class 1 (spike-and-wave).

	Mean	std	Variance	Bounds
Class 0	1.446e+06	4.235e+06	1.794e+13	[9.46e+02, 3.162+e07]
Class 1	4.32e+06	7.892e+06	6.228e+13	[2.715e+03, 4.321e+07]

Table 4. Mean, standard deviation, variance and bound values for median $(\widetilde{x}_t)$ for class 0 (non-spike-and-wave) and class 1 (spike-and-wave).

	Mean	std	Variance	Bounds
Class 0	1.089e+03	1.002e+04	1.004e+08	[-2.769e+04, 2.179e+04]
Class 1	-6.125e+03	2.672e+04	7.140e+08	[-7.325e+04, 7.406e+04]

To illustrate the above point, figure 4 shows a 3D scatter plot of the feature vector for spike-and-wave events (SWD, class 1, red dots) and non-spike-and-wave events (non-SWD, class 0, blue dots). One observes that the SWD events tend to be more dispersed compared to non-SWD events. This is corroborated by Figure 5 that shows the parameters in pairs, with the following combinations

1. Scale parameter (ς_t) vs variance (σ_t^2): for class 1 (SWD), one observes a direct relationship between the variance and sigma, where both parameters grow proportionally. For class 0 (non-SWD), both sigma and variance remain in a limited range of values.
2. Scale parameter (ς_t) vs median $(\widetilde{x}_t)$: as sigma grows, median increases then decreases for both SWD and non-SWD, but is larger for SWD. A cone-shaped pattern can be observed.
3. Variance (σ_t^2) vs median $(\widetilde{x}_t)$: as the variance grows, the median increases then decreases for SWD, while it remains in a small range (cluster) for non-SWD.

The performance of our 10-nearest neighbors classifier was evaluated using a dataset consisting of 96 samples, separate from the training set. These samples were extracted from six EEG signals from subjects different from those used for training. We assessed the total accuracy of the classification. The proposed method achieved a 95 % sensitivity (True positive rate), 87% specificity (True Negative Rate), and 92% accuracy.

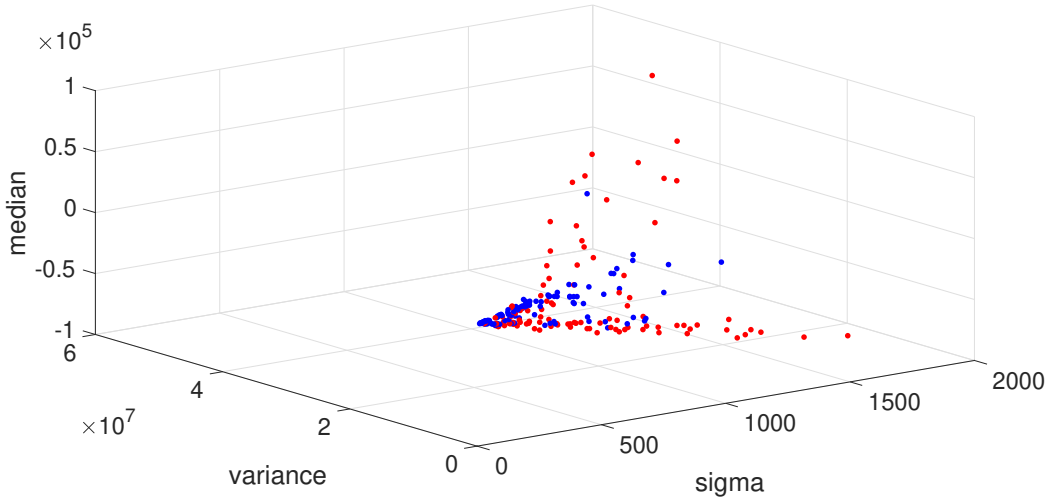

Figure 4. 3D scatter plot of the feature vector $[\varsigma, \sigma_t^2, \widetilde{x}_t]$ for class 0 (non-spike-and-waves events, blue dots), and class 1 (spike-and-waves events, red dots). The SWD events tend to be more dispersed than non-SWD events.

Preprints (www.preprints.org) | NOT PEER-REVIEWED | Posted: 29 October 2020 doi:10.20944/preprints202010.0616.v1

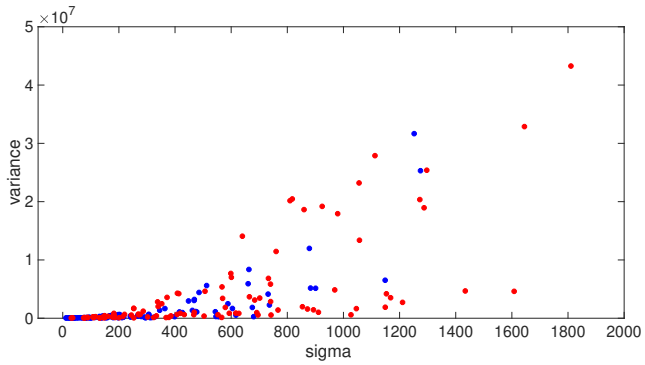

(a) sigma (ς_t) vs variance (σ_t^2)

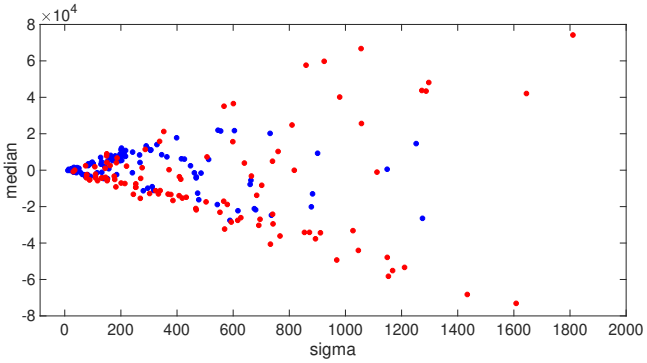

(b) sigma (ς_t) vs median ($\widetilde{x}_t$)

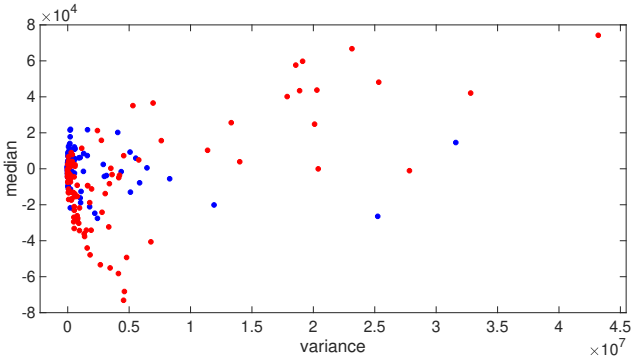

(c) variance (σ_t^2) vs median ($\widetilde{x}_t$)

Figure 5. Scatter plots of the signals used for training, with ς_t, σ_t^2, and $\widetilde{x}_t$ parameters class 0 (non-spike-and-waves events, blue dots), and class 1 (spike-and-waves events, red dots), showing the data dispersion of the proposed approach. In (**a**) Scale parameter (ς_t) vs variance (σ_t^2). For class 1 (SWD), we can see the direct relationship between the variance and sigma, both grow proportionally, while for class 0 (non-SWD) both sigma and variance remain in a range of values. (**b**) Scale parameter (ς_t) vs median ($\widetilde{x}_t$). As sigma grows, the median increases then decreases for both SWD and non-SWD, but is larger for SWD. (**c**) variance (σ_t^2) vs median ($\widetilde{x}_t$). As variance grows, the median increases then decreases for SWD, while it remains in a small range for non-SWD.

4. Discussion

The proposed model-based classification method to detect patient-specific spike-and-wave events in long-term EEG signals is based on three feature parameters (or predictors). These are the *scale* parameter from the generalized Gaussian distribution, see eq. (6), the *variance* and the *median*, all estimated from the continuous Morlet coefficients. These features are used with a 10-nearest neighbors classifier to discriminates spike-and-wave from non-spike-and-wave events. Experimental results with

Preprints (www.preprints.org) | NOT PEER-REVIEWED | Posted: 29 October 2020 doi:10.20944/preprints202010.0616.v1

real data from a hospital achieved 95 % sensitivity (True positive rate), 87% specificity (True Negative Rate), and 92% accuracy. Based on our rule to choose k, the value was $\sqrt{212} \approx 14$, but we found a better performance by choosing empirically $k = 10$. Techniques used in this study are widely known in the scientific community, but they have never before been put together to detect patient-specific epileptiform patterns in EEG. Our main contribution lies in the type of features proposed to detect spike-and-wave patterns and its application to human data. From a technical point of view, the GGD scale parameter depends on the shape parameter, see eq. (5) and Tables 2 to 4. They can therefore not be used together as features. Using only the scale parameter would restrict the representation space leading to pour representation of natural variability in the data. We therefore augmented the representation space by considering the variance and the median of wavelet coefficients. This choice has proven pertinent to discriminating SWD patterns from non-SWD.

The data collection protocol consisted of a neurologist selecting ten SWD patterns for each patient to be part of the training database. Our hypothesis was that using multiple signal patterns from individual patients improves the classification. This enhances learning patient-specific patterns, leading to precise detection of epileptiform pattern compared to previous work [39].

The collected dataset was previously used with other methods (see Table 5). We can see that the proposed method doesn't provide significantly more precise results . However, it has the advantage of analyzing the EEG signal in the time-frequency domain, where previous methods were based on temporal waveform characterization. On the other hand, the assumption that the data has a generalized Gaussian distribution allows a strong dimension reduction, leading to low computational solution relying on rigorous statistical properties.

Table 5. Results form other methods applied to the same dataset in percent (%), in terms of TPR = True Positives Rate or Sensitivity; TNR = True Negative Rate or Specificity; FPR = False positive Rate; ACC = Accuracy: and high Specificity, rule in (SpPIn). Training and testing have different numbers of patients due to different research settings.

Method	Features	Classifier	TPR	TNR	ACC	Training	Testing	Ref.
GGD	GGD parameters, variance and median from time-frequency Morlet wavelet decomposition	10-NN	95	87	92	212	96	Actual
Kendall's Tau-b Coefficient	Kendall's Tau-b coefficient significance in time domain	SpPIn	-	94	94	300	300	[39]
TLS	TLS parameters in time domain	1-NN	100	100	100	192	46	[20]
Cross-correlation	Correlation coefficient in time domain	Decision trees	86	98	97	96	46	[9]

5. Conclusions

This paper presented a new model-based classification method to detect spike-and-wave events in long-term EEG signals in humans. The proposed method is based on the scale parameter of the generalized Gaussian distribution augmented with the variance and the median of the continuous Morlet wavelet coefficients from EEG data and a k-nearest neighbors classification technique.

The performance of the method was evaluated by training the model with an annotated real dataset containing 212 signal recordings consisting of spike-and-wave and non-spike-and-wave events. The classification performance was assessed utilizing 96 segments and achieved 95 % sensitivity (True positive rate), 87% specificity (True Negative Rate), and 92% accuracy. These results set the path to potentially new research to study the causes underlying the so-called *absence epilepsy* in long-term EEG recordings.

In addition to its performance, the proposed method can be implemented in online epilepsy care applications. However, due to the high dynamics of the EEG epileptic signals, some waveform might

 doi:10.20944/preprints202010.0616.v1

be incomplete (with part of the signal missing due to artefacts). Our method is not able to detect such situations, as confirmed by physicians using visual inspection [39]. Future work will focus on other epileptic waveform patterns as well as on the extensive evaluation of the proposed approach and its comparison with other methods from the literature both in humans and rodents. Other techniques, such as visual data analysis with t-distributed stochastic neighbor embedding [51] and deep learning variational autoencoders [52] will be considered. For future clinical research, an on-line user interface will be implemented with different functionalities such as automatic SWD detection and SWD pattern counts for each brain region.

Author Contributions: Conceptualization, Antonio Quintero-Rincón, Valeria Muro and Hadj Batatia; Formal analysis, Antonio Quintero-Rincón and Hadj Batatia; Investigation, Antonio Quintero-Rincón, Valeria Muro and Hadj Batatia; Methodology, Antonio Quintero-Rincón and Jorge Prendes; Software, Antonio Quintero-Rincón; Validation, Antonio Quintero-Rincón, Valeria Muro, Carlos D'Giano and Hadj Batatia; Visualization, Antonio Quintero-Rincón, Valeria Muro, Carlos D'Giano and Hadj Batatia; Writing-original draft, Antonio Quintero-Rincón and Jorge Prendes; Writing-review & editing, Antonio Quintero-Rincón, Valeria Muro, Carlos D'Giano, Jorge Prendes and Hadj Batatia

Funding: This research received no external funding.

Acknowledgments: Part of the work was conducted by AQR during his Ph.D. work at Buenos Aires Institute of Technology (ITBA). We would also like to thank the Bioengineering Ivana Zorgno for her assistance in the writing.

Conflicts of Interest: The authors declare no conflict of interest.

Abbreviations

The following abbreviations are used in this manuscript:

EEG	Electroencephalography
FLENI	Fight against Pediatric Neurological Disease
GGD	Generalized Gaussian distribution
k-NN	k-nearest neighbors
SWD	Spike-and-wave discharge

References

1. Donald L. Schomer and Fernando Lopes da Silva *Niedermeyer's Electroencephalography Basic Principles, Clinical Applications, and Related Fields.*; LWW, 2010.
2. Bergstrom, R.; Choi, J.; Manduca, A.; Shin, H.; Worrell, G.; Howe, C. Automated identification of multiple seizure-related and interictal epileptiform event types in the EEG of mice. *Scientific Reports* **2013**, *3*.
3. Bhuyan, R.; Jahan, W.; Upadhyaya, N. Interictal wave pattern study in EEG of epilepsy patients. *International Journal of Research in Medical Sciences* **2013**, *5*, 3378–3384.
4. Quintero-Rincón, A.; Pereyra, M.; D'Giano, C.; Batatia, H.; Risk, M. A new algorithm for epilepsy seizure onset detection and spread estimation from EEG signals. *Journal of Physics: Conference Series* **2016**, *705*, 012032.
5. Gajic, D.; Djurovic, Z.; Gennaro, S.D.; Gustafsson, F. Classification of EEG signals for detection of epileptic seizures based on wavelets and statistical pattern recognition. *Biomedical Engineering: Applications, Basis and Communications* **2014**, *26*, 1450021.
6. Navakatikyan, M.; Colditz, P.; Burke, C.; Inder, T.; Richmond, J.; Williams, C. Seizure detection algorithm for neonates based on wave-sequence analysis. *Clinical Neurophysiology* **2006**, *117*, 1190–1203.
7. Siuly, S.; Kabir, E.; Wang, H.; Zhang, Y. Exploring sampling in the detection of multicategory EEG signals. *Computational and Mathematical Methods in Medicine* **2015**, *576437*.
8. Subasi, A.; Ercelebi, E. Classification of EEG signals using neural network and logistic regression. *Computers Methods and Programs in Biomedicine* **2005**, pp. 87–99.
9. Quintero-Rincón, A.; Alanis, M.; Muro, V.; D'Giano, C. Spike-and-Wave detection in epileptic signals using cross-correlation and decision trees. *Revista Argentina de Bioingeniería, Bioengineering Argentinian Society* **2018**, *21*, 1–4.

10. Donos, C.; Dumpelmann, M.; Schulze-Bonhage, A. Early Seizure Detection Algorithm Based on Intracranial EEG and Random Forest Classification. *International Journal of Neural Systems* **2015**, *5*, 1550023.
11. Fu, R.; Tian, Y.; Shi, P.; Bao, T. Automatic Detection of Epileptic Seizures in EEG Using Sparse CSP and Fisher Linear Discrimination Analysis Algorithm. *Journal of Medical Systems* **2020**, pp. 1–13.
12. Ossadtchi, A.; Greenblatt, R.E.; Towle, V.L.; Kohrman, M.H.; Kamada, K. Inferring spatiotemporal network patterns from intracranial EEG data. *Clinical Neurophysiology 121* **2010**, *122*, 823–835.
13. Wilson, S.B.; Emerson, R. Spike detection: A review and comparison of algorithms. *Clinical Neurophysiology* **2002**, *113*, 1873–1881.
14. Hese, P.V.; Martens, J.; Waterschoot, L.; Boon, P.; Lemahieu, I. Automatic detection of spike and wave discharges in the EEG of genetic absence epilepsy rats from Strasbourg. *IEEE Transactions on Biomedical Engineering* **2009**, *56*, 706–717.
15. Pearce, P.; Friedman, D.; Lafrancois, J.; Iyengar, S.; Fenton, A.; Maclusky, N.; Scharfman, H. Spike wave discharges in adult Sprague Dawley rats and their implications for animal models of temporal lobe epilepsy. *Epilepsy and Behavior* **2014**, *32*, 121–131.
16. M Le Van Quyen, J.F.; Lachaux, J.; Rodriguez, E.; Lutz, A.; Martinerie, J.; Varela, F.J. Comparison of Hilbert transform and wavelet methods for the analysis of neuronal synchrony. *Journal of Neuroscience Methods* **2001**, *111*, 83–98.
17. Puspita, J.W.; Gunadharma, A.I.J.S. Classification of epileptiform and wicket spike of EEG pattern using backpropagation neural network. *AIP Conference Proceedings* **2017**, *1825*, 020018.
18. Gupta, A.; Singh, P.; Karlekar, M. A Novel Signal Modeling Approach for Classification of Seizure and Seizure-Free EEG Signals. *IEEE Transactions on Neural Systems and Rehabilitation Engineering* **2018**, *5*, 925–935.
19. Quintero-Rincón, A.; D'Giano, C.; Batatia, H. A quadratic linear-parabolic model-based EEG classification to detect epileptic seizures. *The Journal of Biomedical Research* **2020**, *3*, 203–210.
20. Quintero-Rincón, A.; Prendes, J.; Muro, V.; D'Giano, C. Study on Spike-and-wave detection in epileptic signals using t-location-scale distribution and the k-nearest neighbors classifier. *IEEE URUCON Congress on Electronics, Electrical Engineering and Computing* **2017**, *2017*, 1–4.
21. Li, P.; Karmakar, C.; Yearwood, J.; Venkatesh, S.; Palaniswami, M.; Liu, C. Detection of epileptic seizure based on entropy analysis of short-term EEG. *PLoS One* **2018**, *3*, e0193691.
22. Jirka, J.; Prauzek, M.; Krejcar, O.; Kuca, K. Automatic epilepsy detection using fractal dimensions segmentation and GP-SVM classification. *Neuropsychiatric Disease and Treatment* **2018**, *14*, 2439–2449.
23. Paul, Y. Various epileptic seizure detection techniques using biomedical signals: a review. *Brain Informatics.* **2018**, *5*, 1–19.
24. Subasi, A.; Alkana, A.; Koklukayab, E.; Kiymik, M.K. Analysis Of Epileptic Seizure. Detection Methods Based on Parameter Estimation, Power Spectrum Density And Morlet Wavelet Transform. *Neural Networks* **2005**, *18*, 985–997.
25. Xanthopoulos, P.; Liu, C.C.; Zhang, J.; Miller, E.R.; Nair, S.P.; Uthman, B.M.; Kelly, K.; Pardalos, P.M. A robust spike and wave algorithm for detecting seizures in a genetic absence seizure model. *Annual International Conference of the IEEE Engineering in Medicine and Biology Society* **2009**, pp. 2184–2187.
26. Sitnikova, E.; Hramov, A.E.; Koronovsky, A.A.; van Luijtelaar, G. Sleep spindles and spike-wave discharges in EEG: Their generic features, similarities and distinctions disclosed with Fourier transform and continuous wavelet analysis. *Journal of Neuroscience Methods* **2009**, *180*, 304–316.
27. Richard, C.D.; Tanenbaum, A.; Audit, B.; Arneodo, A.; Khalil, A.; Frankel, W. SWDreader A Wavelet-Based Algorithm Using Spectral Phase to Characterize Spike-Wave Morphological Variation in Genetic Models of Absence Epilepsy. *Journal of Neuroscience Methods* **2014**, *242*, 127–140.
28. Pollen, D.A. Intracellular studies of cortical neurons during thalamic induced wave and spike. *Electroencephalography and Clinical Neurophysiology* **1964**, *17*, 398–404.
29. Ovchinnikov, A.; Luttjohann, A.; Hramov, A.; van Luijtelaar, G. An algorithm for real-time detection of spike-wave discharges in rodents. *Journal of Neuroscience Methods* **2010**, *94*, 172–178.
30. Rodgers, K.; Dudek, F.; Barth, D. 2. Progressive, Seizure-Like, Spike-Wave Discharges Are Common in Both Injured and Uninjured Sprague-Dawley Rats: Implications for the Fluid Percussion Injury Model of Post-Traumatic Epilepsy. *Journal of Neuroscience* **2015**, *35*, 9194–9204.
31. Blumenfeld, H. Cellular and Network Mechanisms of Spike-Wave Seizures. *Epilepsia* **2005**, *46*, 21–33.

32. Avoli, M. A brief history on the oscillating roles of thalamus and cortex in absence seizures. *Epilepsia* **2012**, *53*, 779–789.
33. Puspita, J.W.; Gunadharma, S.; Indratno, S.W.; Soewono, E. Bayesian approach to identify spike and sharp waves in EEG data of epilepsy patients. *Biomedical Signal Processing and Control* **2017**, *35*, 63–69.
34. Zhu, J.D.; Lin, C.F.; Chang, S.H.; Wang, J.H.; Peng, T.I.; Chien, Y.Y. Analysis of spike waves in epilepsy using Hilbert-Huang transform. *Journal of Medical Systems* **2014**, *39*, 1–13.
35. Medvedeva, T.M.; Sysoeva, M.V.; Luijtelaa, G.; Sysoev, I.V. Modeling spike-wave discharges by a complex network of neuronal oscillators. *Archives of Psychiatry and Clinical Neuroscience* **2018**, *98*, 271–282.
36. Olejarczyk, E.; Rudner, R.; Marciniak, R.; Wartak, M.; Stasiowski, M.; Jalowiecki, P.; Sobieszek, A. Detection of the EEG spike-wave patterns evoked by volatile anaesthetics. *IFMBE Proceedings* **2009**, *25*, 407–409.
37. Zibrandtsen, I.C.; Nielsen, J.M.; Kjaer, T.W. Quantitative characteristics of spike-wave paroxysms in genetic generalized epilepsy. *Clinical Neurophysiology* **2020**, *131*, 1230–1240.
38. Haghighi, H.S.; Markazi, A.H. Dynamic origin of spike and wave discharges in the brain. *NeuroImage* **2019**, *197*, 69–79.
39. Quintero-Rincón, A.; Carenzo, C.; Ems, J.; Hirschson, L.; Muro, V.; D'Giano, C. Spike-and-wave epileptiform discharge pattern detection based on Kendall's Tau-b Coefficient. *Applied Medical Informatics* **2019**, *1*, 1–8.
40. Tenneti, S.V.; Vaidyanathan, P.P. Absence Seizure Detection Using Ramanujan Filter Banks. *52nd Asilomar Conference on Signals, Systems, and Computers* **2018**, pp. 1913–1917.
41. Polivannyi, F.; Igasaki, T.; Neshiger, N.M.R. Wavelet Transform-Based Algorithm for Single Spike-and-Wave Discharges Detection in Epileptic Patients' Electroencephalogram. *8th International Conference on BioMedical Engineering and Informatics* **2015**, pp. 255–259.
42. Quintero-Rincón, A.; Prendes, J.; Pereyra, M.; Batatia, H.; Risk, M. Multivariate Bayesian Classification of Epilepsy EEG Signals. *IEEE 12th Image, Video, and Multidimensional Signal Processing Workshop (IVMSP)* **2016**, pp. 1–5.
43. Quintero-Rincón, A.; Pereyra, M.; D'Giano, C.; Batatia, H.; Risk, M. A visual EEG epilepsy detection method based on a wavelet statistical representation and the Kullback-Leibler divergence. *IFMBE proceedings, Springer Singapore* **2017**, *60*, 13–16.
44. Quintero-Rincón, A.; Pereyra, M.; D'Giano, C.; Risk, M.; Batatia, H. Fast statistical model-based classification of epileptic EEG signals. *Biocybernetics and Biomedical Engineering* **2018**, *38*, 877–889.
45. Ahuja, N.; Lertrattanapanich, S.; Bose, N. Properties determining choice of mother wavelet. *IEE Proceedings - Vision, Image and Signal Processing* **2005**, *152*, 659–664.
46. Abry, P. *Ondelettes et turbulence. Multirésolutions, algorithmes de décomposition, invariance d'échelles*; Diderot Editeur, Paris., 1997.
47. Do, M.N.; Vetterli, M. Wavelet-Based Texture Retrieval Using Generalized Gaussian Density and Kullback-Leibler Distance. *IEEE Transactions on Image Processing* **2002**, *11*, 146–158.
48. Quintero-Rincón, A.; D'Giano, C.; Risk, M. Epileptic seizure prediction using Pearson's product-moment correlation coefficient of a linear classifier from generalized Gaussian modeling. *Neurología Argentina* **2018**, *10*, 201–217.
49. Bishop, C.M. *Pattern Recognition and Machine Learning (Information Science and Statistics)*; Springer-Verlag New York, Inc., 2006.
50. Barber, D. *Bayesian Reasoning and Machine Learning.*; Cambridge University Press., 2012.
51. van der Maaten, L..; Hinton, H.. Visualizing Data using t-SNE. *Journal of Machine Learning Research* **2008**, *9*, 2579–2605.
52. Zemouri, R.; Lévesque, M; Amyot, N.; Hudon, C.; Kokoko,O. Deep Variational Autoencoder: an efficient tool for PHM frameworks. *Prognostics and Health Management Conference (PHM-Besancon)* **2020**, 235–240.